Chapter 4
Correlated Single-Nanoparticle Calculations and Measurements

Preface

The content that appears in this chapter has been largely adapted from the following publications:

McMahon JM, Wang Y, Sherry LJ, Van Duyne RP, Marks LD, Gray SK, Schatz GC (2009) Correlating the Structure, Optical Spectra, and Electrodynamics of Single Silver Nanocubes. J Phys Chem C 113:273–2735. doi:10.1021/jp8098736

Ringe E, McMahon JM, Sohn K, Cobley C, Xia Y, Huang J, Schatz GC, Marks LD, Van Duyne RP (2010) Unraveling the Effects of Size, Composition, and Substrate on the Localized Surface Plasmon Resonance Frequencies of Gold and Silver Nanocubes: A Systematic Single-Particle Approach. J Phys Chem C 114: 12511–12516

The experimental work that appears in this chapter was done by Wang Y, Sherry LJ, Ringe E, Sohn K, Cobley C, Xia Y, Huang J, Marks LD, and Van Duyne RP. Although, the experimental aspects are not discussed heavily, and the reader interested in such details is referred to Refs. [1–3].

4.1 Introduction

In Chap. 1, it was stated that the purpose of science is to describe the phenomena of nature. In this chapter, the question of how well can one correlate computational modeling with experiments at the nanoscale is addressed. In order to do this, experimental single-nanoparticle data (both optical responses and structural information) must be available [3–5], and a completely correlated computation and measurement must be made. This can be done by using structural information from experimental high-resolution transmission electron microscopy (HRTEM) measurements (which can resolve subnanometer features and has $\sim$10,000 times higher magnification capabilities than optical microscopy) in an FDTD simulation,

J. M. McMahon, *Topics in Theoretical and Computational Nanoscience*, Springer Theses, DOI: 10.1007/978-1-4419-8249-0_4,

which can then be compared with experimental LSPR spectroscopy measurements of the same nanoparticle. (In addition, three-dimensional and internal crystallographic structural information can be obtained by using HRTEM via various techniques, such as electron energy loss spectroscopy and diffraction.)

This chapter describes fully correlated computations and measurements of Ag nanocubes (Au nanocubes are briefly discussed as well), which are used to determine how well classical EM applies at the nanoscale. This chapter also explores the relationship between particle morphology, substrate composition, and LSPR spectral position(s) for these systems. The relative merits of the JC [6] and LH [7] Ag dielectric data for describing perfect crystalline nanoparticles are also addressed.

4.2 Computational Considerations

The calculations in this section were performed using FDTD as outlined in Sect. 3.2. Computational domains were discretized using grid spacings of 1.0 nm in all directions for the Ag nanocubes and 0.5 nm for the Au nanocubes, and terminated with CPML. The dielectric functions of Ag, Au, and carbon (C) were approximated using the D2L model fit to empirically determined dielectric data [6–8] over wavelengths important to this study ($\lambda = 300-800\,\text{nm}$); Appendix B. Plots of these fits, which will be relevant later, are shown in Fig. 4.1. Formvar and glass were both modeled using a constant RI of $n = 1.5$.

4.3 Correlation of Computation and Experiment

Colloidal Ag nanocubes were synthesized, and a correlated LSPR spectrum and HRTEM image of a single nanocube was obtained [3]; Fig. 4.2. From the HRTEM image, the face-to-face widths are found to be 85.6(5) and 80.9(5) nm along both in-plane directions, with two of the corners rounded to 11.0(5) nm radii of curvature and the other two rounded to 12.0(5) nm. The structural information available from this image is limited by the HRTEM resolution and the top-down perspective. However, a cube height of 83(1) nm can be assumed by taking the average of the in-plane face-to-face widths, and the radii of curvature of the bottom edges and corners can be inferred from the corresponding top corners.

Two main peaks are observed in the LSPR spectrum, a narrow peak at 399 nm and a broad peak at 461 nm. The assignment of these peaks has been analyzed in detail previously [9], where it was demonstrated that they are resonances associated with the tips of the nanocube, where the EM fields are the most intense. Two peaks result from the two dielectric environments present, and have adiabatic correlations with the dipole and quadrupole resonances of the cube in a homogeneous environment. By analogy to the corresponding resonances for spherical or

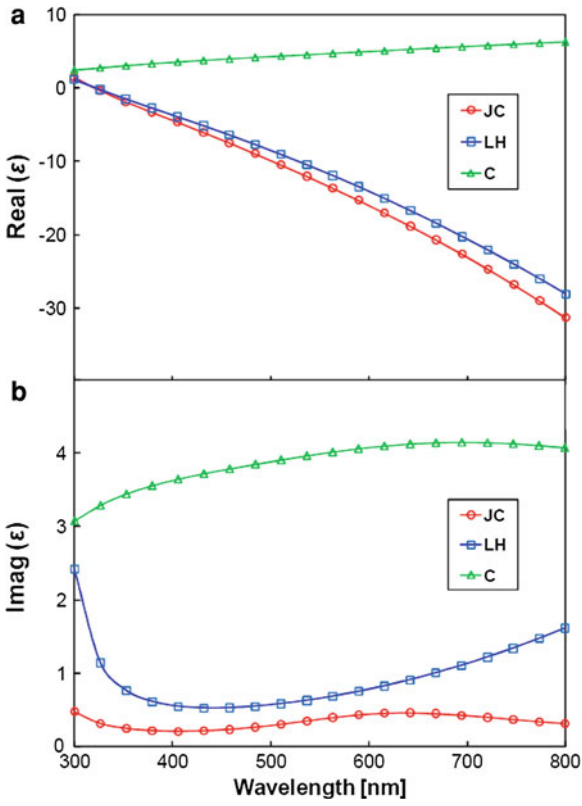

Fig. 4.1 **a** Real and **b** imaginary parts of the Ag (JC and LH) and C dielectric constants, evaluated using Eq. 2.23 with parameters from Appendix B

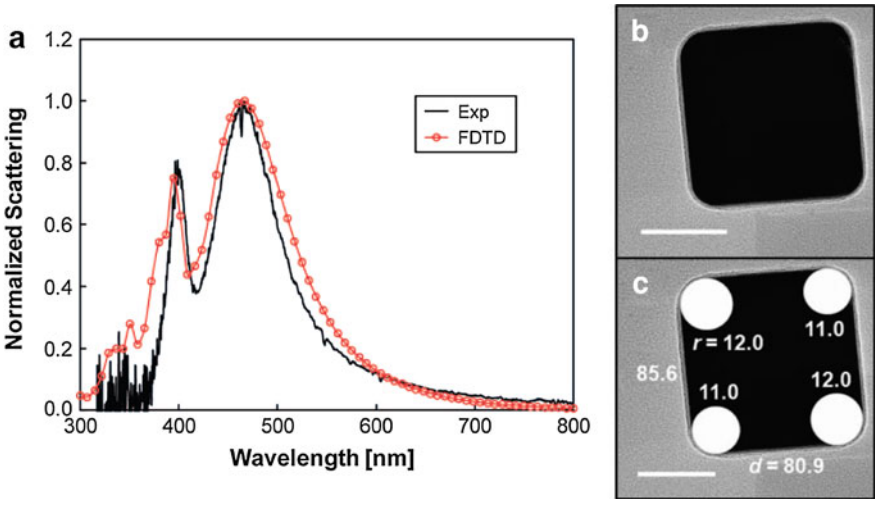

Fig. 4.2 Correlated LSPR–HRTEM measurement of a single Ag nanocube: **a** LSPR spectrum, **b** HRTEM image, and **c** same as **b** with overlaid structural parameters (in nm). The *inset white scale bars* in **b** and **c** represent 40 nm; the FDTD calculated scattering cross section is also shown in **a** with open *red circles*

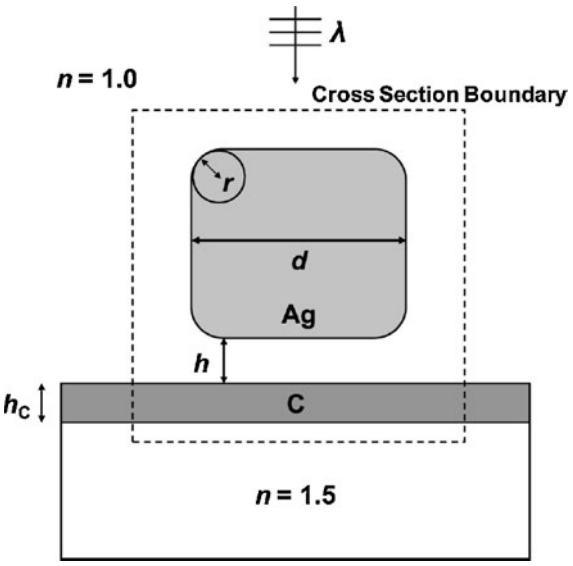

Fig. 4.3 Two-dimensional schematic diagram of the nanocube system modeled with FDTD. The parameters in the figure are defined in the text

spheroid-shaped particles, the dipole resonance is expected to be broader than the latter due to important radiative damping effects [10]. Figure 4.2a shows that this analogy holds for the cube resonances, with the linewidth of the higher wavelength peak being 2.03 times that of the lower wavelength one (experimental). Of course, other effects can also contribute to the linewidths, such as charge transfer processes between the particle and its surrounding medium (so-called "chemical interface damping" effects [11]). However, in the present application, the widths of the peaks seem to be well accounted for by electrodynamics calculations in which the particle and surrounding media are described using bulk dielectric constants; see Sect. 4.4.4.

For the FDTD calculations, the Ag nanocube was defined by its dielectric constant (JC or LH), face-to-face width (d), and radii of curvature of the corners and sides (r). Even though in the experiment each face-to-face width and radius of curvature of a corner or side is slightly different, for simplicity they were assumed identical for the calculations (which should not affect any of the presented results). The nanocube was spaced by a distance h from a C layer with thickness h_C. The C layer was placed on an infinite $n = 1.5$ substrate, and the surrounding medium was air $(n = 1.0)$. Figure 4.3 shows a two-dimensional schematic diagram of the described system. Scattering cross sections using normal incident illumination were calculated for comparison with the experimental LSPR spectrum. Even though in the experiment the cube is illuminated at an angle, and light is only collected for a range of angles around the forward direction [1], past studies of these effects indicate that calculations and experiment should nonetheless have similar LSPR spectra.

The scattering cross section of a nanocube with a face-to-face width of $d = 83\,\text{nm}$ and $r = 13\,\text{nm}$ of rounding, spaced $h = 2\,\text{nm}$ above an $h_C = 2\,\text{nm}$ thick C

layer, and modeled with JC dielectric data is shown in Fig. 4.2a, where excellent agreement with experiment is seen. The nanocube in this calculation was positioned at $h = 2$ nm above the C layer to simulate the effect that it may not be resting directly on the substrate. This spacing could arise from physisorbed or weakly chemisorbed water, carbon dioxide, and hydrocarbons on the substrate, as well as citrate, oxygen, and possibly hydroxyls on the nanocube surface. Depending on the thickness and dielectric constant of adsorbed molecules, the LSPR positions and linewidths will be affected, so other choices of h are considered below. Unfortunately, there is no way to estimate the dielectric constant(s) of this, so in the rest of this chapter it is taken to be 1.0.

4.4 System Parameters

To determine the effects that the nanocube parameters and local dielectric environment have on the optical response, as well as to determine if such parameters can be considered "free" to use to fit calculations to experiment, further FDTD calculations were carried out.

4.4.1 Face-to-Face Width

Scattering cross sections calculated for nanocubes modeled using the LH dielectric data with face-to-face widths of $d = 80$ and 90 nm and no corner rounding are compared to experiment in Fig. 4.4a. These parameters were chosen to elucidate only the effect due to the face-to-face width, and are at the extremes of the actual parameters seen in the HRTEM image (Fig. 4.2c). The $d = 80$ nm nanocube is seen to agree better with experiment, with the higher and lower wavelength peaks 21 and 10 nm closer to the experimental values, respectively. The difference in shifts is related to the smaller dielectric sensitivity of the lower wavelength (more quadrupolar) mode compared to the higher wavelength (more dipolar) mode, as found previously for other particle shapes [12]. This effect arises from the shorter range of the near-field decay of the lower wavelength mode. However, even for the $d = 80$ nm nanocube, the calculated lower and higher wavelength peak positions are 35 and 44 nm redshifted from the experimental values, respectively. Such discrepancy arises from the choice of parameters other than the face-to-face width, which also have a large effect on the positions of both peaks and their relative amplitudes (see the other sections below).

4.4.2 Corner Rounding

Scattering cross sections calculated for a $d = 80$ nm nanocube with corners and sides rounded to various radii of curvature and compared to experiment are shown in Fig. 4.4b. In addition, to increase the dielectric substrate sensitivity, the

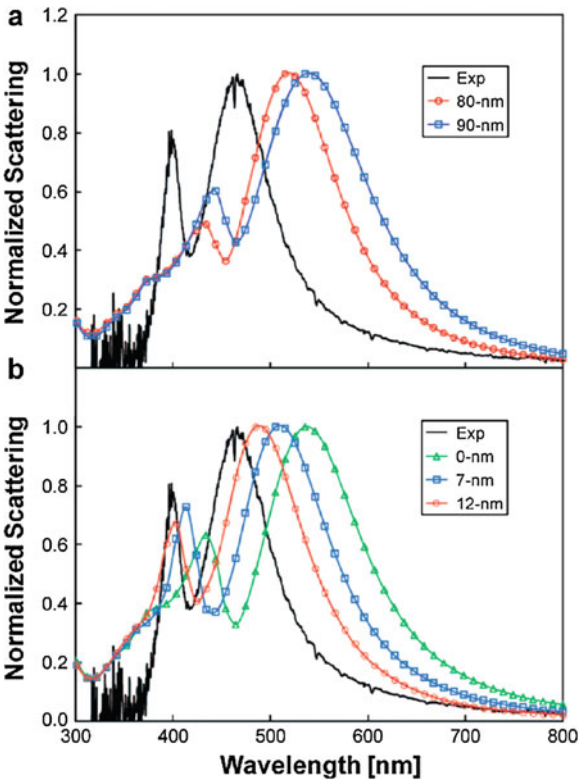

Fig. 4.4 FDTD calculated scattering cross sections of a Ag nanocube in response to **a** the variation in the face-to-face width, with no corner rounding and placed $h = 2$ nm above the C layer, and **b** the variation in the radii of curvature of the corners and sides of a $d = 80$ nm nanocube placed $h = 1$ nm above the C layer. In both cases, the nanocube was modeled with the LH dielectric data, and the C layer was $h_C = 2$ nm thick

nanocube was moved to $h = 1$ nm above the C layer. The FDTD calculations show that the higher wavelength peak shifts by 41 nm as the radii increase from $r = 0$ to 12 nm, whereas the lower wavelength peak only shifts by 29.5 nm. These results are again related to the dielectric sensitivity of the quadrupolar mode versus the dipolar one, and they highlight the importance of the near-field contact area in determining the dielectric response of the nanocube, as has been found previously for other particle shapes [13].

4.4.3 Substrate Effect

Additional insight concerning the effect of the C layer is provided by scattering cross sections calculated with the nanocube placed directly on the substrate, with and without C present; Fig. 4.5. For these calculations, the contact area was made large by using a $d = 90$ nm nanocube with only $r = 7$ nm rounding, and the effect of C was heightened by making the layer $h_c = 3$ nm thick. The results show that the C layer has little effect on the lower wavelength peak, but redshifts and significantly damps the higher wavelength one. This is again related to the fact that

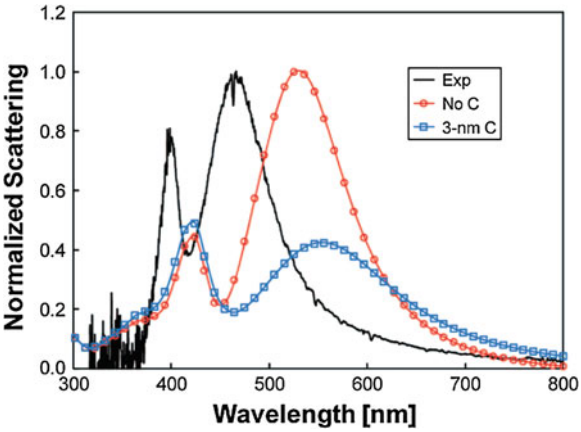

Fig. 4.5 FDTD calculated effect of the C layer on a $d = 90$ nm Ag nanocube. The nanocube was modeled with the LH dielectric data, has corners and sides rounded to $r = 7$ nm radii of curvature, and was placed directly on the substrate (with or without the C layer)

the near-field decay of the lower wavelength mode is much shorter than the higher wavelength one, and is therefore relatively unaffected by the substrate. These findings demonstrate the exquisite sensitivity of LSPR properties to substrate position and dielectric response, a result previously demonstrated by using gold nanorings [14]. Additionally, this demonstrates that the optimal parameters that were chosen to compare to experiment (Sect. 4.3) are unique.

4.4.4 Empirical Dielectric Data Sets

To assess the relative merits of the JC and LH Ag dielectric data when used to model perfect crystalline nanoparticles (such as the nanocubes in this chapter), scattering cross sections of a $d = 90$ nm nanocube with $r = 7$ nm rounding were calculated to compare to experiment for both sets of data; Fig. 4.6. For these calculations, there was no C layer, and the nanocube was placed directly on the $n = 1.5$ substrate. It is seen that the JC data gives results that agree much better with experiment, with the lower and higher wavelength peaks 10 and 21 nm closer to the experimental values, respectively. In addition, the JC dielectric data more accurately describes the width and relative amplitude of the lower wavelength peak.

Both the JC and LH dielectric data sets are inferred from thin films that are presumably polycrystalline or somewhat amorphous in character. It is therefore not a priori obvious why the JC dielectric data best describes the perfect crystalline nanocubes discussed here. However, it has been found that for crystalline Ag nanowires, the LH dielectric data provides a too lossy of description, and effectively reducing the loss (more consistent with the JC dielectric data) improves agreement with experiment [15]. Similar conclusions were also obtained in studies of Ag nanostrips made using electron-beam methods [16].

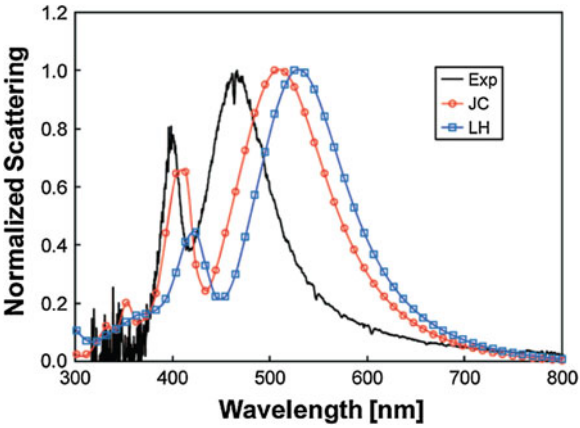

Fig. 4.6 Comparison of the JC to LH Ag dielectric data for modeling perfect crystalline nanoparticles, using a $d = 90$ nm nanocube as the example. The nanocube has corners and sides rounded to $r = 7$ nm radii of curvature and was placed directly on a $n = 1.5$ RI substrate with no C layer

4.5 Summary and Outlook

The discussion in this chapter shows that by carefully correlating computations and experimental measurements, near perfect agreement can be obtained. Additionally, for large nanostructures (i.e., those composed of many hundreds of thousands of atoms, or more), classical electrodynamics applied with bulk dielectric data is sufficient to describe the novel phenomena that arise. However, care must be taken in selection of the empirical dielectric data set to use, as it was demonstrated that the JC Ag dielectric data is more accurate for describing perfect crystalline nanoparticles compared to that of LH.

By varying structural parameters, the FDTD calculations showed strong sensitivity between the nanocube optical response and the face-to-face width, corner and side rounding, and the substrate. These results impose strict requirements on determination of such parameters (~ 1 nm resolution) if calculation and experiment are to match, and demonstrate that there are no "free parameters" (at least, geometric) that can be used in the simulations. These results are also beneficial for understanding of the relationship between optical response, structure, and dielectric environment of single nanoparticles. For example, the near-field contact area between a nanoparticle and its substrate was demonstrated to be particularly influential on the optical response.

Before ending this chapter, it should be noted that the results presented are not particular to the studied system (a Ag nanocube), nor should the following results be indicative that these results are particular only to nanocubes. Recently, similar correlated computations and measurements of Au nanocubes on Formvar and silicon nitride (Si_3N_4, a semiconductor) substrates were made that support the presented claims [2]. (Note that the Formvar substrate was similar to the one used in this chapter, except that the C layer was placed down, such that the nanocube was not in near-field contact with it. Additionally, for the calculations, Si_3N_4 was taken to have a constant RI of $n = 2.0$.)

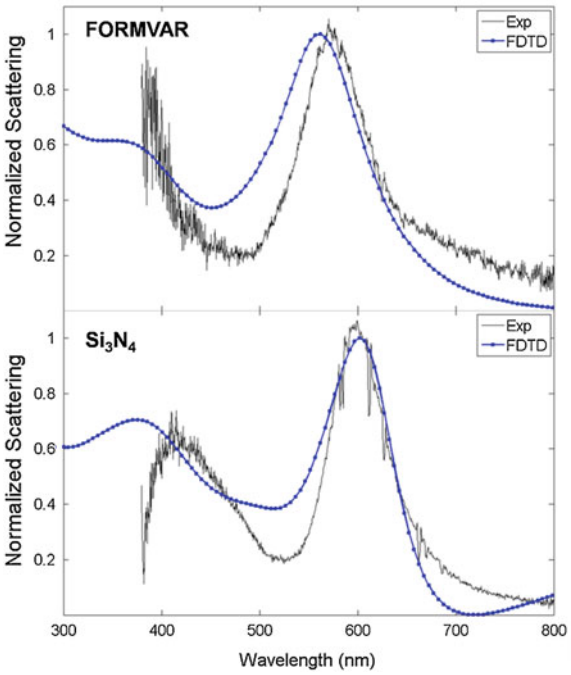

Fig. 4.7 Comparison of FDTD calculated *blue line with symbols* and experimental *solid black line* scattering from isolated Au nanocubes on *top* Formvar and *bottom* Si_3N_4. Structural information from HRTEM measurements was used in the FDTD calculations; the experimental spectra were obtained using correlated HRTEM–LSPR measurements

Using HRTEM, experimental nanocube parameters were obtained: for the Formvar substrate, $d = 84.0\,\text{nm}$ and $r = 15.2\,\text{nm}$, and for the Si_3N_4 one, $d = 74.2\,\text{nm}$ and $r = 12.7\,\text{nm}$. By using these parameters in FDTD calculations, excellent agreement with the experiments were again obtained; Fig. 4.7. However, for the nanocube on Formvar, the calculated dipolar LSPR appears 10 nm to the blue of the experimental one. This can be attributed to the fact that the FDTD calculations assume that there are no contaminants on the surface of the nanocube, which could possibly create a higher local dielectric environment, leading to a redshift in the experimental result. This would not have as significant of an effect on the Si_3N_4 results, where the substrate RI is already high (much like the small C layer in the Ag nanocube results).

References

1. McMahon JM, Wang Y, Sherry LJ, Van Duyne RP, Marks LD, Gray SK, Schatz GC (2009) Correlating the structure, optical spectra, and electrodynamics of single silver nanocubes.J Phys Chem C 113:2731–2735
2. Ringe E, McMahon JM, Sohn K, Cobley C, Xia Y, Huang J, Schatz GC, Marks LD, Van Duyne RP (2010) Unraveling the effects of size, composition, and substrate on the localized surface plasmon resonance frequencies of gold and silver nanocubes: a systematic single-particle approach. J Phys Chem C 114:12511–12516

3. Wang Y, Eswaramoorthy SK, Sherry LJ, Dieringer JA, Camden JP, Schatz GC, Van Duyne RP, Marks LD (2009) A method to correlate optical properties and structures of metallic nanoparticles. Ultramicroscopy 109:1110–1113
4. Scherer NF, Pelton M, Jin R, Jureller JE, Liu M, Kim HY, Park S, Guyot-Sionnest P (2006) Optical nonlinearities of metal nanoparticles: Single-particle measurements and correlation to structure. P Spie 6323:632309/1–632309/6
5. Mock JJ, Barbic M, Smith DR, Schultz DA, Schultz S (2002) Shape effects in plasmon resonance of individual colloidal silver nanoparticles. J Chem Phys 116:6755–6759
6. Johnson PB, Christy RW (1972) Optical constants of the noble metals. Phys Rev B 6:4370–4379
7. Lynch DW, Hunter WR (1985) Comments on the optical constants of metals and an introduction to the data for several metals. In: Palik ED (ed) Handbook of optical constants of solids, Academic Press, Orlando, pp 275–368
8. Arakawa ET, Dolfini SM, Ashley JC, Williams MW (1985) Arc-evaporated carbon films: optical properties and electron mean free paths. Phys Rev B 31:8097–8101
9. Sherry LJ, Chang SH, Schatz GC, Van Duyne RP, Wiley BJ, Xia Y (2005) Localized surface plasmon resonance spectroscopy of single silver nanocubes. Nano Lett 5:2034–2038
10. Kelly KL, Coronado E, Zhao LL, Schatz GC (2003) The optical properties of metal nanoparticles: the influence of size, shape, and dielectric environment. J Phys Chem B 107:668–677
11. Hovel H, Fritz S, Hilger A, Kreibig U, Vollmer M (1993) Width of cluster plasmon resonances: bulk dielectric functions and chemical interface damping. Phys Rev B 48:18178–18188
12. Sherry LJ, Jin R, Mirkin CA, Schatz GC, Van Duyne RP (2006) Localized surface plasmon resonance spectroscopy of single silver triangular nanoprisms. Nano Lett 6:2060–2065
13. Malinsky MD, Kelly KL, Schatz GC, Van Duyne RP (2001) Nanosphere lithography: effect of substrate on the localized surface plasmon resonance spectrum of silver nanoparticles. J Phys Chem B 105:2343–2350
14. Larsson EM, Alegret J, Käll M, Sutherland DS (2006) Sensing characteristics of NIR localized surface plasmon resonances in gold nanorings for application as ultrasensitive biosensors. Nano Lett 7:1256–1263
15. Laroche T, Vial A, Roussey M (2007) Crystalline structure's influence on the near-field optical properties of single plasmonic nanowires. Appl Phys Lett 91:123101
16. Drachev VP, Chettiar UK, Kildishev AV, Yuan HK, Cai W, Shalaev VM (2008)The Ag dielectric function in plasmonic metamaterials. Opt Express 16:1186–1195